



pubs.acs.org/estengg

Scalable Reactor Design for Electrocatalytic Nitrite Reduction with **Minimal Mass Transfer Limitations**

Chenxu Yan, Sruthi Kakuturu, Ashley Hesterberg Butzlaff, David M. Cwiertny, Syed Mubeen, and Charles J. Werth*



Cite This: https://dx.doi.org/10.1021/acsestengg.0c00054



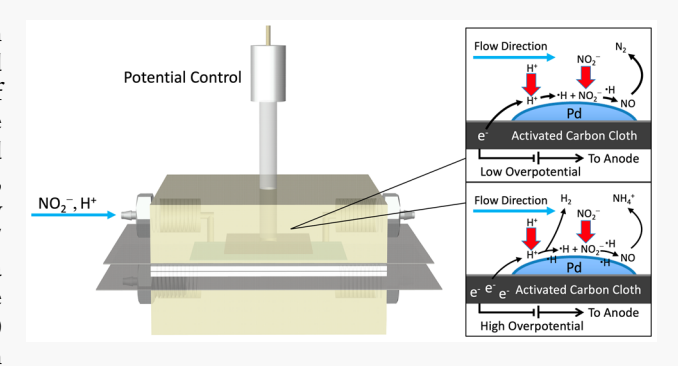
ACCESS

Metrics & More

Article Recommendations

Supporting Information

ABSTRACT: A parallel-plate thin-layer (PPTL) flow reactor with potential control and custom-made cathode of Pd-In modified activated carbon cloth was developed for electrocatalytic removal of nitrite from water; the effect of applied potential and flow rate were investigated. Compared to other reactors in the literature, rapid nitrite reduction (first-order rate constant is 0.38 L g_{pd}^{-1} min⁻¹), high current efficiency (CE, 51%), and low ammonium selectivity (5.4%) were observed at an applied potential of -0.60 V vs the Ag/ AgCl reference electrode (RE) and a flow rate of 40 mL min⁻¹ in a phosphate buffer solution of pH 6.5. Slightly faster kinetics were observed at more negative potentials (0.57 L g_{Pd}^{-1} min⁻¹ at -1.0 V/RE), but then ammonium production (88%), H2 gas evolution



 $(E_0 = -0.61 \text{ V/RE})$, and current loss (CE < 10%) became problematic. Nitrite reduction was measured in the PPTL flow reactor for almost 50 2 h cycles over six months, with little apparent loss (30%) in activity. A reactive transport model was developed and used to simulate the kinetic data. The fitted intrinsic rate constant (k_w) was 5.2×10^{-6} m s⁻¹, and ratios of dimensionless Nusselt numbers to reaction rate constant values support the reactor being more reaction than mass transfer limited. Application of the parametrized model demonstrated how the PPTL reactor could be scaled (e.g., cathode dimensions, flow channel thickness), operated (i.e., flow rate), or modified (i.e., greater intrinsic catalyst activity) to most efficiently remove nitrite from larger flow streams.

KEYWORDS: Nitrite reduction, Electrocatalytic reduction, Flow reactor design, Mass transfer, Reactive transport modeling

1. INTRODUCTION

Nitrate (NO₃⁻) is the nation's most ubiquitous groundwater contaminant, mainly resulting from agricultural activities such as the application of ammonium and nitrate-based fertilizers, as well as feedlot runoff. Nitrite (NO₂⁻) often co-occurs with nitrate as a (de)nitrification transformation product. The consumption of nitrate-containing water causes methemoglobinemia in infants,² and in vivo formation of more toxic and carcinogenic NO₂⁻ and N-nitrosamines.³ Therefore, maximum contaminant levels (MCLs) in drinking water for NO₃⁻ and NO₂⁻ are regulated by the U.S. EPA at 10 mg L⁻¹ as nitrogen, and 1 mg L⁻¹ as nitrogen, respectively. The primary method to remove these oxyanions is ion exchange, which only transfers nitrates from one phase to another and produces a concentrated waste brine that must be disposed. Catalytic treatment has emerged as a promising alternative to destroy nitrates and minimize waste products. Proposed pathways for catalytic NO₃⁻ reduction are presented in Scheme 1, built on the research first reported in 1989. Facile NO₃ reduction to NO2 usually requires a platinum group metal (PGM), a promoter metal (e.g., In, Cu, Sn), and an electron donor, which in most studies is atomic hydrogen generated at the PGM catalyst from a supply of hydrogen gas. 5,6 NO₃ is first

Scheme 1. Proposed Reaction Pathways for Catalytic

$$NO_{3}^{-} \xrightarrow{Pd - M} NO_{2}^{-} \xrightarrow{Pd} NO \text{ (ads)} \xrightarrow{Pd} N_{2}O \xrightarrow{Pd} N_{2}$$

$$M = In, Cu, Sn$$

$$M = In_{3} Cu, Sn$$

$$M = In_{4} Cu, Sn$$

reduced to NO2- by the promoter metal. Atomic hydrogen generated at the PGM then spills over onto the promoter metal and reduces the metal back to its original valency. Subsequent reduction steps to either dinitrogen gas (N_2) or ammonium (NH₄⁺) as the end product only require the PGM and the atomic hydrogen. End product selectivity toward N₂ is favored by factors that increase the density of nitrogen species on PGM surfaces, and therefore the probability of N-N

Received: June 29, 2020 Revised: October 27, 2020 Accepted: November 2, 2020



pairing,⁵ for example, higher nitrate or nitrite and lower hydrogen concentrations,^{5,7,8} stronger sorption of nitrate reduction intermediates at lower pH,^{5,7-10} and preferential sorption of nitrogen over hydrogen species on select catalysts.^{5,11,12}

Catalytic nitrate and nitrite reduction experiments in batch reactors typically measure fast intrinsic reaction rates provided an excess hydrogen supply, rapid mixing to minimize boundary layer mass transfer limitations near catalyst surfaces, and fast intraparticle mass transfer with small particle sizes (e.g., <26.1 μm^{11}). However, slow H₂ mass transfer can limit reaction rates in practically useful flow-through reactors like fixed bed flow-through reactors. ^{13–21} One of the most efficient was a trickle bed reactor whose overall reaction rates were at the highest 18% of reaction rates in batch mode due to H₂ mass transfer limitations. ^{20,21} More recent alternative membrane reactors with embedded catalyst particles were developed to enhance hydrogen mass transfer to catalyst particles. ^{10,22–25} While mass transfer was shown to be improved, optimization in operational parameters like flow rate and catalyst metal deposition is needed to further improve overall reaction rates in those

More recently, electrocatalytic reduction has shown promise to address hydrogen mass transfer shortcoming via direct charge transfer to nitrates with conductive electrode materials, 26-30 or hydrogenation of nitrates by hydrogen generation with protons and supplied electrons at a PGM electrode.³⁰⁻³⁴ With direct charge transfer to nitrates, the overpotential required is usually high, and H₂ evolution may co-occur, which result in poor current efficiency and high energy consumption. With hydrogenation, atomic hydrogen is generated on PGMs at a higher potential (less negative) than molecular hydrogen, which means atomic hydrogen can be used to reduce nitrates with a higher current efficiency because molecular hydrogen losses are avoided. Also, the overpotential for hydrogenation is typically low compared to direct charge transfer, so there is less corrosion. While the concept of an electrocatalytic reactor reducing nitrates using only atomic hydrogen is attractive, a scalable reactor with high transformation rates, efficient current usage, and end-product selectivity has yet to be realized.

Electrocatalytic batch reactors are simple and efficient at the laboratory scale, but off-line treatment and slow mass transfer (due to mixing limitations) impede their application in water treatment plants.³⁵ In contrast, continuous flow reactors allow direct in-line removal of NO₃⁻ and NO₂⁻, making use of a pumping head already provided in a water treatment plant. Several such reactors have been evaluated in the laboratory, but not all are kinetically or energy efficient, and/or scalable. The most studied electrocatalytic flow reactors are termed plate-in-tank reactors in which "widely" spaced electrode plates are vertically submerged in an electrolyte, 36-40 and the flow recirculates between the reactor and an external reservoir. Such reactors lack active mixing, and suffer from mass transport limitations.³⁸ Other reactor configurations designed to reduce mass transfer limitations are a fluidized bed with inert particles between electrode plates, ^{27,38} and a packed or vertically moving bed with cathodically active particles. ^{38,41,42} However, the former (fluidized bed) demonstrated only marginally better performance over a plate-in-tank reactor,³⁸ and the latter (catalytic particles) suffers from poor charge circulation and high electron resistance due to insufficient contact between particles or spheres used as the cathode.⁴¹ More recently, a

flow-through reactor with a membrane cathode⁴³ achieved fair to good current efficiency, but the overpotential and energy consumption to reach the optimal removal were high due to solution resistance;⁴³ it was also not clear if this type of reactor could be modified for scale-up.

A promising alternative is the parallel-plate, thin-layer (PPTL) electrochemical reactor (a.k.a. filter press reactor), where flow occurs as thin sheets over reactive electrode surfaces, and the cathode and anode are often separated by a flat-sheet cation exchange membrane. Such reactors are available at large scale and serve many purposes (e.g., chloroalkali synthesis, heavy metal removal, and organic contaminant removal).44 Nitrate and nitrite reduction have been investigated in PPTL reactors designed for operation in galvanostatic mode (i.e., controlled current). 45-50 This approach operates and scales simply, but compromises current efficiency and end-product selectivity because hydrogen gas evolution (and associated nitrogen hydrogenation to ammonium) cannot be minimized via potential control. This has limited the application of this promising reactor design in water treatment.

The objectives of this study are to design a new scalable PPTL reactor with potential control to maximize NO₂ reduction rates, current efficiency, and selectivity for the N₂ end product. While NO₃⁻ is the primary contaminant of concern, NO2 is the first intermediate and is chosen as an ideal probe compound to evaluate reactor performance independent of promoter metal characteristics. The reactor was designed with a custom cathode that is fabricated from a porous 3-D activated carbon cloth with Pd and In metal catalysts deposited via incipient wetness method. The reactor was evaluated under different applied potentials and flow rates for NO₂⁻ reduction activity, selectivity, current efficiency, and energy consumption. A longevity test was also carried out to evaluate the reliability of the reactor system. A convectiondiffusion-reaction-recirculation model was developed and conceptualized the cathodic chamber as two parallel-plate ducts with a first-order reaction occurring on a surface in the middle of the two ducts coupled with a recirculation system. It uniquely integrates a known semianalytical solution to the convection-diffusion-reaction equation with a mass balance for recirculation. The model was applied to simulate the experimental data, to acquire the intrinsic reaction rate constant, and to distinguish kinetic reaction versus mass transfer effects on the overall reaction rates. The parametrized model was then used to determine how cathode dimensions, flow channel thickness, intrinsic catalyst activity, and flow rate affect reactor scale-up.

2. EXPERIMENTAL METHODS

2.1. Reagents. $Pd(NO_3)_2 \cdot 2H_2O$ (~40% Pd basis; Sigma-Aldrich) and $In(NO_3)_3 \cdot H_2O$ (99.999% metal basis, Alfa Aesar) were used as the metal precursors for catalyst deposition on the carbon cloth electrode. $NaNO_2$ (99%; Sigma-Aldrich) was the nitrite source. KH_2PO_4 (99%; Sigma-Aldrich) and K_2HPO_4 (98%; Sigma-Aldrich) were used to prepare the buffer solution and control pH in reduction experiments. HNO_3 (70%, TraceMetal grade, Fisher Scientific) was used for digestion prior to inductively coupled plasma optical emission spectroscopy (ICP-OES) analysis to determine the catalyst loadings on the carbon cloth. All solutions were prepared in ultrapure water (18.2 $M\Omega \cdot cm$) produced by a Barnstead Nanopure system (Thermo Fisher Scientific).

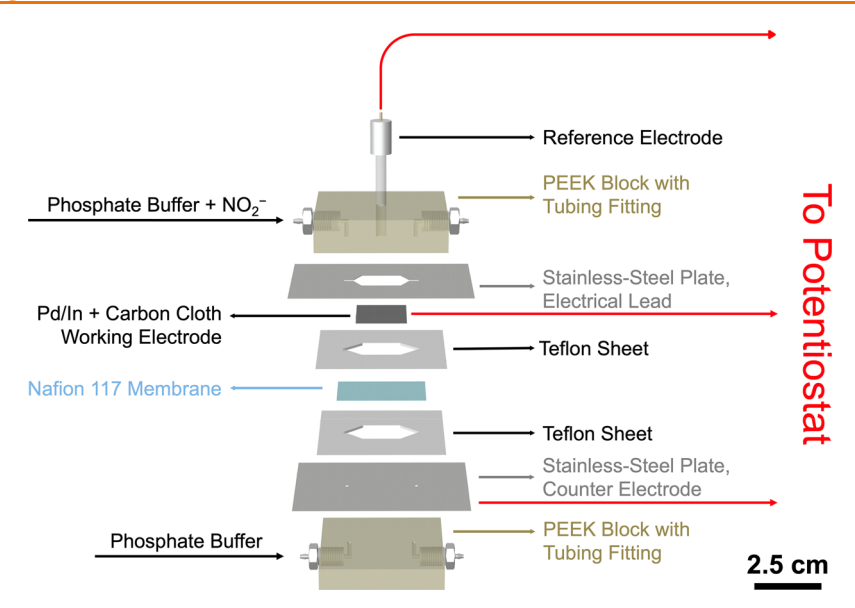


Figure 1. A schematic of the parallel-plate thin-layer flow reactor for electrocatalytic nitrite reduction. In reduction experiments, the reactor operates in recirculation mode. Catholyte and anolyte solutions are circulated through cathodic and anodic chambers using a peristaltic pump, respectively, from two individual reservoirs, each containing 40 mL of solution. The scale bar represents 2.5 cm.

2.2. Cathode Catalyst Preparation. Kynol activated carbon cloth (ACC-5092-10) was obtained from Gun EI Chemical Industry (Japan), hereafter referred to as ACC. Pd and In were deposited via incipient wetness method ^{11,43,51} on a piece of ACC (Pd–In/ACC) that was cut to 2.5 cm \times 2.0 cm ($L \times W$; \sim 0.1800 g). Details are provided in the Supporting Information (SI).

2.3. Nitrite Reduction Experiments. 2.3.1. Electrocatalytic Reactor Design. A parallel-plate thin-layer (PPTL) flow reactor for electrocatalytic nitrite reduction was developed and is shown in Figure 1. It consists of two compartments, each approximately 1 cm³ in volume. The top one contains the cathodic chamber, and consists of a polyetheretherketone (PEEK) block sitting on a 0.2 mm thick stainless-steel plate fixed to a piece of Pd-In/ACC with 1 mm thick flow cavities on either side (or a piece of only ACC in a set of control experiments). The stainless-steel plate with the Pd-In/ACC is the working electrode, and is connected to a potentiostat. The PEEK block has holes on the sides that serve as inlet and outlet ports to direct the flow over and under the stainless-steel sheet with the working electrode. The PEEK block also has a hole drilled from the top that houses the reference electrode (RE), and positions it directly above the working electrode to reduce solution resistance. The reference electrode is Ag/AgCl in 1.0 M KCl (E_{RE} = 0.222 V/SHE, CH Instrument, Inc.) in all experiments. The 1 mm thick flow chamber directly above the Pd-In/ACC sheet is created in the stainless-steel sheet, sealed to the PEEK block by a thin layer of polydimethylsiloxane (PDMS); the flow chamber directly below the working electrode is machined into a Teflon sheet.

The bottom compartment of the flow reactor contains the anodic chamber, and it is separated from the cathodic chamber by a 0.183 mm thick Nafion 117 (Chemours) membrane. The Nafion membrane allows only cations to diffuse through, so that nitrite and its reduction products are inhibited in passing from the cathode to the anode and being oxidized. A possible exception is the cation $\mathrm{NH_4}^+$. However, a study showed $\mathrm{NH_4}^+$ transport across the membrane is slow compared to the time scale of the experiments. S2 We also did not detect significant

 $\mathrm{NH_4}^+$, nitrate, or nitrite in the anodic solution. The bottom compartment is almost a mirror image of the top compartment; it consists of another PEEK block underlying a 0.2 mm thick stainless-steel plate and a 1 mm thick Teflon sheet. The stainless-steel sheet serves as the counter electrode without an affixed carbon cloth, and the PEEK block does not have the reference electrode housing. Thin PDMS gaskets are placed between each layer, and the entire assembly is pressed together and sealed using an external metal frame. The reactor operates in continuous flow mode, either once-through or in recirculation mode.

2.3.2. PPTL Flow Reactor Nitrite Reduction Experiments. The PPTL flow reactor was operated in recirculation mode. A 40 mL solution initially containing 100 mg L⁻¹ nitrite and 1.0 M phosphate buffer (pH 6.5 \pm 0.1, 1:1 molar ratio of KH₂PO₄ and K₂HPO₄, degassed under a vacuum for 15 min before use) was pumped into the cathodic chamber of the reactor while another 40 mL solution with only 1.0 M phosphate buffer was pumped into the anodic chamber of the reactor. The effluent from both chambers was circulated back to their respective reservoirs and well mixed with their remaining solution using a magnetic stir bar. The 1.0 M phosphate buffer was selected over other buffer systems (i.e., 0.1 M phosphate buffer with and without constant CO2 bubbling) to ensure a relatively constant solution pH during reactions (Table S1). The 1.0 M phosphate buffer did not significantly inhibit the catalytic activity compared to 0.1 M phosphate buffer (Figure S1), which was used for catalytic nitrite reduction in our previous study.⁵³ CO₂ bubbling was not preferred since catalytic activity was inhibited (Figure S1), possibly due to electrocatalytic CO₂ reduction reaction (CO₂RR) competing with nitrite reduction when carbonate species were present. 54,55 A Gamry 1010E potentiostat (Warminster, PA) was connected to the reactor and a desired potential drop was applied between the assynthesized Pd-In/ACC working electrode and the reference electrode. The reaction was performed for 2 h while the current on the working electrode was recorded. Samples were taken regularly from the cathodic reservoir for the analysis of NO₂⁻ and NH₄⁺ concentrations. The NO₂⁻ reduction

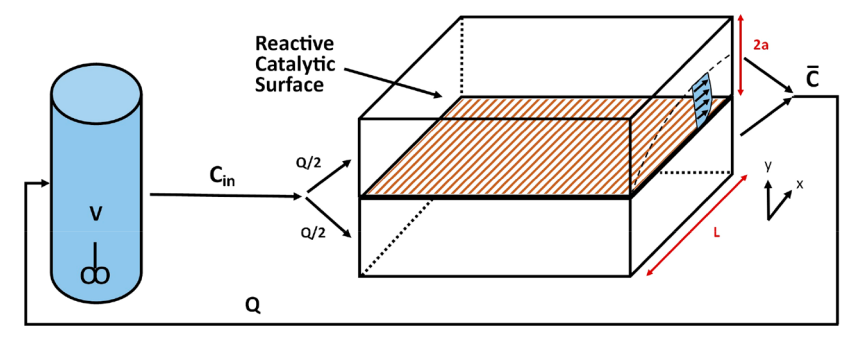


Figure 2. A simplified schematic of the full reactor system that was modeled with laminar flow.

Table 1. Parameters and Values Used in the Reactive Transport Model

parameter	definition	value
x	spatial coordinates parallel to the flow direction	
y	spatial coordinates perpendicular to the flow direction ^a	
\overline{x}	dimensionless coordinates parallel to the flow direction	
\overline{y}	dimensionless coordinates perpendicular to the flow direction ^a	
C_{i}	mass concentration of i	
$C_{i,in}$	inlet mass concentration of i	
\overline{C}_i	dimensionless concentration of species i	
$\overline{C}_{i, \text{in}}$	dimensionless inlet concentration of species i	
$egin{array}{c} C_{i, ext{in}} \ \overline{C}_i \ \overline{C}_{i, ext{in}} \ \overline{C}_{i, ext{avg}}(\overline{x}) \ \overline{C}_{i, ext{avg}} \end{array}$	dimensionless concentration of i averaged over the y direction at any location \overline{x}	
$\overline{C}_{i,avg}$	dimensionless concentration of i averaged over the y direction at the end of x	
D	effective diffusion coefficient of $\mathrm{NO_2}^{-b}$	$2.03 \times 10^{-9} \text{ m}^2 \text{ s}^{-1}$
a	one-half distance between the noncatalytic plate and the catalytic wall	0.0005 m
L	length of the catalytic wall	0.024 m
ν	mass average velocity	$8.33 \times 10^{-4} \text{ m s}^{-1} \text{ to } 3.33 \times 10^{-2} \text{ m s}^{-1c}$
V	reservoir volume	$4.0 \times 10^{-5} \text{ m}^3$
Q	volumetric flow rate	$8.33 \times 10^{-9} \text{ m}^3 \text{ s}^{-1} \text{ to } 3.33 \times 10^{-7} \text{ m}^3 \text{ s}^{-1c}$
β_n	eigenvalues of the nth mode	
γ_n	normalized eigenfunctions	
$k_{ m w}$	intrinsic reaction rate constant for a first-order reaction	
$K_{ m w}$	dimensionless reaction rate constant	$K_{\rm w} \equiv \frac{k_{\rm w}a}{D}$
k_m	mass transfer coefficient	
Nu	dimensionless mass transfer coefficient	$\text{Nu} \equiv \frac{k_m a}{D} = \frac{\sum_{n=1}^{n=\infty} \beta_n^2 \gamma_n^2 e^{-\beta_n^2 \overline{x}}}{\frac{3}{4} \sum_{n=1}^{n=\infty} \gamma_n^2 e^{-\beta_n^2 \overline{x}} - \frac{1}{K_w} \sum_{n=1}^{n=\infty} \beta_n^2 \gamma_n^2 e^{-\beta_n^2 \overline{x}}}$
$K_{ m E}$	overall dimensionless reaction rate constant	$K_{\rm E} \equiv \frac{1}{\frac{1}{K_{\rm W}} + \frac{1}{{\rm Nu}}} = \frac{\sum_{n=1}^{n=\infty} \beta_n^2 \gamma_n^2 e^{-\beta_n^2 x}}{\frac{3}{4} \sum_{n=1}^{n=\infty} \gamma_n^2 e^{-\beta_n^2 \overline{x}}}$

[&]quot;The origin of y or \overline{y} axis is defined as the middle point between the noncatalytic plate and the catalytic wall. ^bCalculated from Wilke-Change equation. ^cFlow rates used in the experiments (i.e., 1 mL min⁻¹ to 40 mL min⁻¹) are divided in half because each parallel-plate duct has half of the total flow.

experiments were performed at different potentials (-0.40, -0.60, -0.80, -1.0 V/RE) and flow rates (1, 5, 20, 40, 100 mL min⁻¹) to evaluate NO₂⁻ reduction performance. Experiments performed with different Pd–In/ACC cloth pieces at 100 mL min⁻¹ gave inconsistent results, which are provided in Figure S4.

2.3.3. Analytical Methods of NO₂⁻ and NH₄⁺. Nitrite concentrations were analyzed using ion chromatography (IC, Dionex ICS-2100) equipped with a Dionex IonPac AS19 column. The eluent was KOH solution (20–45 mM), and the flow rate was 1 mL min⁻¹. Ammonium concentrations were determined using Hach colorimetric kits (TNT 832, 2–47 mg L⁻¹ NH₄⁺–N, salicylate method).

2.4. Electrode Characterization. The elemental analysis of the Pd–In/ACC was carried out using concentrated HNO₃ digestion followed by ICP-OES analysis as described in the SI. Powder X-ray diffraction (PXRD) patterns of the ACC and the Pd–In/ACC were collected on a Rigaku R-axis Spider diffractometer (Cu source) operating at 40 kV and 40 mA. An image of catalyst metals deposited on the Pd–In/ACC was collected using an FEI Tecnai transmission electron microscope (TEM) operating at 80 kV. The TEM sample was prepared by drop-casting an ethanolic dispersion of fibers from the Pd–In/ACC on a 200-mesh copper grid (Cu/Formvar; Ted Pella) and allowing for complete evaporation of ethanol. Current–potential behavior of the working electrode was characterized using multistep chronoamperometry (CA).

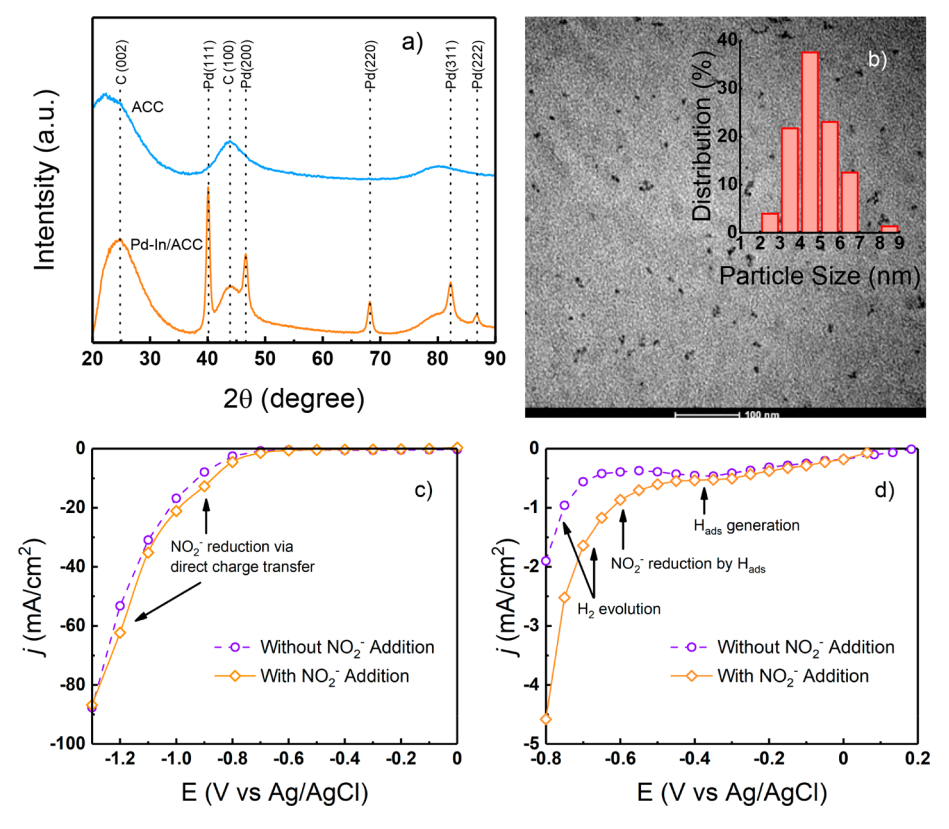


Figure 3. (a) PXRD patterns of the ACC and the Pd–In/ACC. The dashed lines represent the locations of the characteristic peaks of Pd, In and C. (b) TEM image of catalyst metal particles deposited on the Pd–In/ACC. The inset shows the particle size distribution. (c) Current–potential curves of Pd–In/ACC in 1.0 M phosphate buffer and with 15 mM nitrite addition at 40 mL min⁻¹ in the PPTL flow reactor, with a potential range from –1.3 V/RE to 0 V/RE. (d) Current–potential curves of Pd–In/ACC in 1.0 M phosphate buffer and with 15 mM nitrite addition at 40 mL min⁻¹ in the PPTL flow reactor, with a potential range from –0.80 V/RE to OCP. Arrows indicate the locations where certain reactions are interpreted as occurring.

Through-plane conductivity (σ , S m⁻¹) of the ACC without catalyst deposition and the Pd–In/ACC were determined using electrochemical impedance spectroscopy (EIS). Details are provided in the SI.

2.5. Reactive Transport Modeling. A reactive transport model was used to assess intrinsic reactivity versus mass transfer limitations on overall NO2 reduction rates for the experimental reactor design, and to evaluate performance of a larger-scale reactor. A simplified schematic of the full system that was modeled is illustrated in Figure 2. The anodic chamber was not included in the model as it was only used for completing the circuit. In the cathodic chamber, solution from the reservoir containing NO₂⁻ flows through two parallel-plate ducts where NO₂⁻ reduction occurs as a first-order reaction (observed in kinetics experiments) on the catalytic wall (Pd-In/ACC) in the middle of two ducts. The two ducts are mirror images of each other and the flow in each duct is half of the inlet flow. The two-dimensional concentration profile in each duct was described in a previous model developed by Solbrig and Gidaspow. 56,57 The dimensionless governing equation is given in eq 1:

$$(1 - \overline{y}^2) \frac{\partial \overline{C}_i}{\partial \overline{x}} = \frac{\partial^2 \overline{C}_i}{\partial \overline{y}^2}$$
 (1a)

where

$$\overline{y} = \frac{y}{a}$$
 $\overline{x} = \frac{2xD}{3va^2}$ $\overline{C}_i = \frac{C_i}{C_{i,\text{in}}}$ (1b)

The governing equation is subject to the boundary conditions as described by eq 2:

$$\overline{C}_i(0, \overline{y}) = 1 \tag{2a}$$

$$\frac{\partial \overline{C}_i}{\partial \overline{y}}(\overline{x}, 1) = 0 \tag{2b}$$

$$\frac{\partial \overline{C}_i}{\partial \overline{y}}(\overline{x}, -1) = K_w \overline{C}_i(\overline{x}, -1)$$
(2c)

where

$$K_{\rm w} \equiv \frac{k_{\rm w}a}{D} \tag{2d}$$

The analytical solution for the dimensionless concentration of i ($\overline{C}_{i,\text{avg}}$) averaged over the y direction at any location \overline{x} is shown in eq 3:

$$\overline{C}_{i,\text{avg}}(\overline{x}) = \sum_{n=1}^{\infty} \left(\frac{3}{4}\right) \gamma_n^2 e - \beta_n^2 \overline{x}$$
(3)

Definitions of all parameters are presented in Table 1. Details regarding derivation of the eigenvalues and eigenfunctions are available in the dissertation of Solbrig.⁵⁷

To model the recirculating system, the average dimensionless concentration derived above is combined with a mass balance equation (eq 4) for the 40 mL reservoir, and this was solved numerically with small time increments.

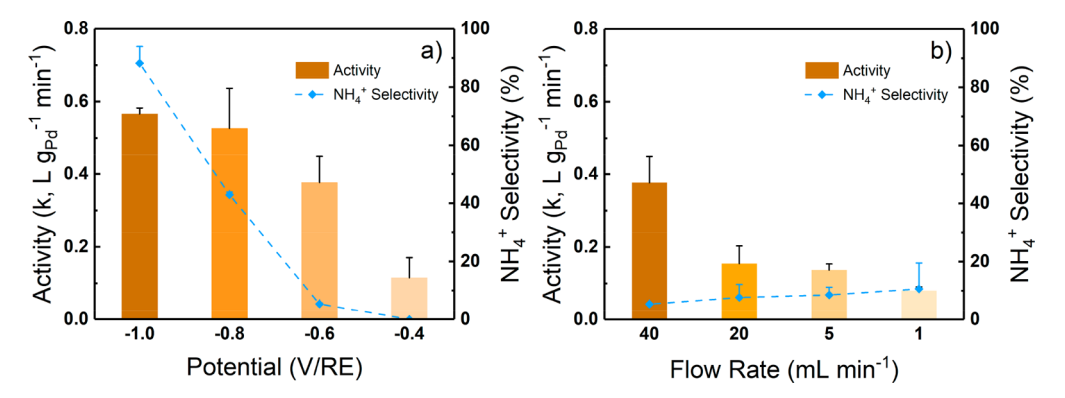


Figure 4. Apparent pseudo-first-order rate constants and NH_4^+ selectivity for electrocatalytic nitrite reduction at (a) different applied potentials at 40 mL min⁻¹, and (b) different flow rates at -0.60 V/RE, in the PPTL reactor. Error bars represent standard deviations.

Table 2. Summary of Nitrite Reduction Results at Different Applied Potentials and Flow Rates in the PPTL Reactor

applied potential (V/RE)	flow rate (mL min ⁻¹)	NO ₂ ⁻ removal (%)	current efficiency (%)	energy consumption (kWh mol ⁻¹ NO ₂ ⁻)	S _{NH₄} (%)
-1.0	40	81 ± 2.5	8.0 ± 0.62	1.9 ± 0.20	88 ± 5.8
-0.80	40	80 ± 7.4	22 ± 1.9	0.41 ± 0.04	43 ± 1.0
-0.60	1	21 ± 3.0	29 ± 4.5	0.19 ± 0.01	11 ± 8.9
-0.60	5	34 ± 3.8	38 ± 2.6	0.14 ± 0.01	8.6 ± 2.6
-0.60	20	38 ± 9.1	37 ± 5.1	0.14 ± 0.02	7.7 ± 4.5
-0.60	40	68 ± 6.9	51 ± 2.8	0.10 ± 0.01	5.4 ± 0.33
-0.40	40	28 ± 11	30 ± 19	0.13 ± 0.08	ND^a
^a Not detected.					

$$V\frac{\mathrm{d}\overline{C}_{i,\mathrm{in}}}{\mathrm{d}t} = Q(\overline{C}_{i,\mathrm{avg}} - \overline{C}_{i,\mathrm{in}}) \tag{4}$$

Thus, the complete model was used to fit all the experimental data at -0.60 V/RE with four different flow rates. $k_{\rm w}$ was the only fitting parameter, and it was adjusted to fit the data at all four flow rates simultaneously. The Nusselt number (Nu) and the overall dimensionless reaction rate constant ($K_{\rm E}$) were calculated to determine the controlling process for NO₂⁻ reduction in the PPTL flow reactor. Nu can be viewed as the dimensionless mass transfer coefficient and $K_{\rm E}$ as the overall reaction rate constant that combines the effect of both reaction kinetics and mass transfer. Accuracy of results for eq 3 was confirmed by comparison to data from Solbrig. ⁵⁷ Different time steps were evaluated to confirm accuracy of the coupled model represented by eq 3 and 4.

3. RESULTS AND DISCUSSION

3.1. Electrode Characterization. The bulk elemental analysis from ICP-OES shows that Pd and In loadings were 0.86 ± 0.18 wt % and 0.07 ± 0.05 wt %, respectively, on the Pd-In/ACC cathode used in all NO₂⁻ reduction experiments. PXRD results for the ACC and Pd-In/ACC, and the characteristic peaks for Pd, In and C, are shown in Figure 3a. The PXRD data for both the ACC and Pd-In/ACC contain characteristic peaks for C(002) and C(100) that are from crystalline carbon in the ACC. In addition, PXRD data for Pd-In/ACC contain characteristic peaks for Pd(111), Pd(200), Pd(220), Pd(311), and Pd(222). Peaks for PdO, In, or In₂O₃ were not found. The PXRD data indicated that the Pd precursors were predominantly reduced to their metallic states with the deposition method used. Indium was not found in the PXRD spectra, possibly because indium concentration is low, or indium appears as amorphous In₂O₃ in the way it is synthesized.51,

The TEM image of the Pd–In/ACC is shown in Figure 3b. It shows a homogeneous distribution of the metal particles on the ACC support with a narrow size distribution of 4.7 \pm 1.1 nm. The through-plane conductivities of the ACC and the Pd–In/ACC were 1.3 S m $^{-1}$ and 1.7 S m $^{-1}$, respectively, similar to electrodes used in other studies. 26,59 The slight increase in conductivity of the Pd–In/ACC compared to the ACC likely resulted from the metal deposition, especially the metallic Pd that was observed from PXRD analysis. The improved conductivity suggests that the deposition of catalyst metals facilitated the application of ACC in the electrocatalytic processes.

The current-potential curves from multistep chronoamperometry between -1.3 V/RE and 0 V/RE are shown in Figure 3c. Two peaks near -0.90 V/RE and -1.2 V/RE, respectively, were observed only after nitrite was added and therefore are attributed to direct nitrite (or nitrite intermediates) reduction on the electrode. Figure 3d provides a closer view in the range from -0.80 V/RE to the open circuit potential (OCP), with and without nitrite addition. Both curves exhibit a peak for H_{ads} generation near -0.40 V/RE and a spike in reductive current starting near -0.65 V/RE due to H₂ evolution. Greater current was observed in the Hads region (approximately between -0.40 V/RE and -0.65 V/RE) when nitrite was added, suggesting greater Hads generation due to its consumption during nitrite reduction. These results indicate that the hydrogenation pathway plays an important role in electroreduction of nitrite, especially at low overpotential (-0.60 V/RE), while direct charge transfer also contributed at more negative potentials.

3.2. Electrocatalytic Nitrite Reduction. Electrocatalytic nitrite reduction experiments were performed at various potentials and flow rates in the PPTL flow reactor. The apparent pseudo-first-order rate constants were obtained from a linear regression of the natural log of $\mathrm{NO_2}^-$ concentration

versus time plots for up to 80% $\mathrm{NO_2}^-$ conversion, and were then normalized to the mass of Pd catalyst (from ICP-OES analysis) on the Pd–In/ACC and the volume of the cathodic solution. The apparent rate constants and $\mathrm{NH_4}^+$ selectivity are shown in Figure 4, while the $\mathrm{NO_2}^-$ removal, current efficiency, energy consumption, and $\mathrm{NH_4}^+$ selectivity are summarized in Table 2. Calculation methods for these key parameters can be found in the SI. The highest rate constant was also normalized to exposed Pd surface area in Table S2, assuming all metal particles within the carbon cloth are accessible to reaction.

3.2.1. Effect of Applied Potentials. Apparent pseudo-firstorder rate constants for NO₂⁻ reduction in the PPTL flow reactor at different applied potentials and a flow rate of 40 mL min⁻¹ are shown in Figure 4a. The highest rate constant (0.57 \pm 0.02 L g_{Pd}^{-1} min⁻¹) and NO₂ removal (81 \pm 2.5%) occurred at -1.0 V/RE. This rate constant is higher than most rate constants in other electrocatalytic NO2- reduction studies. 45,60-62 This rate constant is also comparable to those previously reported for catalytic NO2- reduction in batch experiments using Pd-based catalysts and $\rm H_2$ as the reducing agent. 5,53,63,64 A detailed summary of these rate constants and the reaction time to reduce an 80 mg $NO_2^ L^{-1}$ solution to 40 mg NO₂⁻ L⁻¹ using a 1 g_{metal} L⁻¹ catalyst for (electro)catalytic NO₂⁻ reduction is shown in Table S2. Traditional flow reactors, whether operated in continuous or recirculation mode, are characterized by slow reduction kinetics due to H2 mass transfer limitations, and have rate constants up to 25 times smaller than in batch reactors. 16 Agreement between rate constants for the new PPTL flow reactor and batch experiments indicates efficient nitrite removal and suggests reduced mass transfer limitations.

Apparent rate constants for nitrite reduction in the PPTL flow reactor are similar at -1.0 V/RE and -0.80 V/RE (~ 0.57 L g_{Pd}^{-1} min⁻¹), decrease slightly (i.e., 33%) at -0.60 V/RE, and then decrease sharply at -0.40 V/RE. Significant H₂ gas evolution (bubbles) was only observed at applied potentials below -0.60 V/RE (i.e., at -0.80 V/RE and -1.0 V/RE). Apparent rate constants were also measured using a bare ACC working electrode as a control (Figure S3). It had only 40% of the Pd-In/ACC activity at -1.0 V/RE, almost no activity toward nitrite reduction at -0.60 V/RE, and no observed H₂ gas evolution. Only direct electron transfer likely contributes to nitrite reduction on the bare ACC, based on the lack of a hydrogenation metal and no H2 gas evolution. Therefore, at -1.0 V/RE, the results support both direct charge transfer and hydrogenation of nitrite as possible reaction mechanisms on Pd-In/ACC. This is also supported by chronoamperometry (CA) results, indicating direct nitrite reduction at -0.90 V/RE, and both H_2 and H_{ads} generation below -0.65~V/RE. At -0.80V/RE, the CA results indicate only hydrogenation is possible. However, the equivalence of nitrite reduction rates at -1.0 and −0.80 V/RE suggest contributions from direct charge transfer at -1.0 V/RE are minimal. At -0.60 V/RE, the CA results indicate only H_{ads} and not H_2 is contributing to nitrite reduction. The production rate of H_{ads} may be at least partially responsible for the lower activity at this potential compared to -0.80 V/RE. Finally, at -0.40 V/RE, CA results indicate H_{ads} generation drops sharply, and this is responsible for the large decrease in nitrite reduction activity. Overall, the results indicate that hydrogenation is the dominant reduction pathway at all applied potentials, but at -1.0 V/RE direct charge transfer is possible and may be contributing.

Selectivity for ammonium was determined and is reported in Table 2. It decreases from near 90% to almost zero with applied potential from -1.0 V/RE to -0.40 V/RE, respectively. This decrease corresponds to smaller amounts of reactive hydrogen on the catalyst surface, and is consistent with conventional catalytic studies that found less ammonium is formed when the hydrogen supply is limited. 5,7,8,65-70 This has been attributed to higher coverage of nitrogen species on the catalyst surface at low hydrogen levels, and the greater chance for N-N pairing to occur and form dinitrogen. 5,7,8,65-69 Selectivity for dinitrogen is important in water treatment plants to avoid producing and releasing toxic ammonium to the water distribution system or the environment.

Reduction currents and NO₂⁻ reduction end products were used to calculate current efficiencies, and these are also reported in Table 2. The highest rate constant observed at −1.0 V/RE corresponds to the lowest current efficiency (i.e., 8.0%). This means that less than 10% of the electrons generated were used to reduce nitrite via H_{ads}, while the remaining electrons and the associated energy were wasted most likely through the coupling of Hads to form H2 that escaped from the reactor. Current efficiencies improved when the applied potential was decreased to -0.80 and -0.60 V/RE, reaching 22% and 51%, respectively. At -0.60 V/RE, NO₂removal was only 13% lower than at -1.0 V/RE (i.e., 81% at -1.0 V/RE versus 68% at -0.60 V/RE), and NH_4^+ selectivity was reduced from 88% to 5.4%. Also, the high current efficiency at -0.60 V/RE resulted in the lowest energy consumption at 0.10 kWh $\text{mol}^{-1} \text{ NO}_2^{-}$. At -0.40 V/RE, the NO₂ reduction activity drops off sharply. These results indicate that with careful control of the applied potential, Hads generation on the electrode surface can be controlled and efficiently used for rapid nitrite reduction with minimal energy consumption and ammonium production. This highlights the merit of potential control even though a large number of flow reactors with advective flow (including recirculating system) in the literature and those for large scale applications were operated in the galvanostatic mode; ^{38,45,47–50,71–73} this only regulates the total current circulating through the cathode and anode, and side reactions such as H2 evolution reaction cannot be minimized. 30,48

3.2.2. Effect of Flow Rate. At 40 mL min⁻¹, the applied potential of -0.60 V/RE resulted in relatively fast NO₂ reduction with the lowest energy consumption and ammonium production. Therefore, this applied potential was chosen to probe the effects of flow rates from 1 to 40 mL min⁻¹ on reactor performance. These flow rates correspond to Reynolds numbers from 0.77 to 31, respectively, all in the laminar regime. NO₂ - reduction activity and NH₄ + selectivity as a function of flow rate are presented in Figure 4b. The apparent rate constants increase from 0.08 L g_{Pd}^{-1} min⁻¹ to 0.38 L g_{Pd}^{-1} min⁻¹ when flow rates increase from 1 mL min⁻¹ to 40 mL min⁻¹. The current efficiency follows the same trend and is a maximum at 40 mL min $^{-1}$, while the energy consumption follows the opposite trend. The NH_4^+ selectivity is always below 11%, and is lower at higher flow rates. The trends observed from 1 mL min⁻¹ to 40 mL min⁻¹ are at least partially due to the increased number of recirculation cycles that result from increasing flow rates; at 1 mL min⁻¹ the solution only passes through the reactor twice during the 120 min kinetic run. These trends are also influenced by boundary layer thickness; at higher flow rates this thickness should decrease,

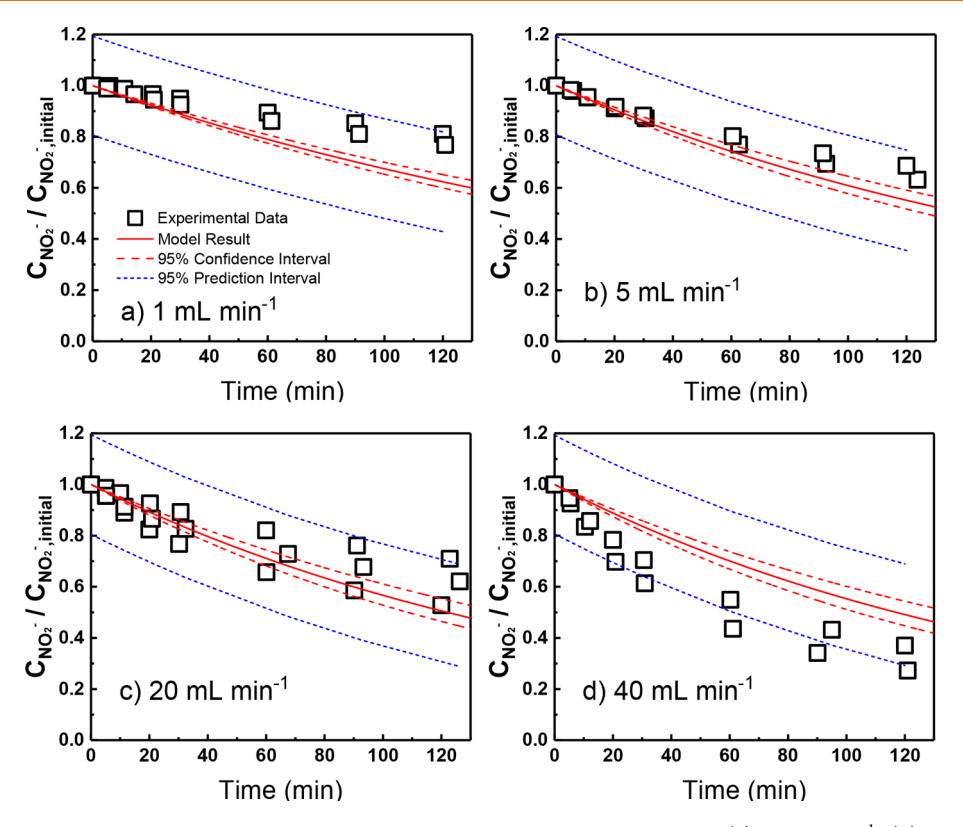


Figure 5. Simulated concentration profiles of nitrite reduction at -0.60 V/RE and a flow rate of (a) 1 mL min⁻¹, (b) 5 mL min⁻¹, (c) 20 mL min⁻¹, and (d) 40 mL min⁻¹ in the PPTL reactor. Black open squares represent experimental data. Red solid and dashed lines represent the concentration profile and its bounds of uncertainty calculated from the fitted k_w value and its 95% confidence intervals, respectively. Blue short dashed lines represent the prediction bounds of new data points with 95% confidence when a separate replicate experiment is to be performed at each flow rate.

thereby improving NO_2^- mass transfer to the cathode surface and possibly overall reaction rates.

3.3. Reactive Transport Modeling of Experiments. A reactive transport model was used to simultaneously fit NO₂ concentration versus time results for the PPTL reactor at four flow rates (i.e., 1-40 mL min⁻¹), all performed at an applied potential of -0.60 V/RE. Model results are shown in Figure 5. Red solid and dashed lines represent the concentration profile and its bounds of uncertainty calculated from the fitted $k_{\rm w}$ value and its 95% confidence intervals, respectively. Blue short dashed lines represent the prediction bounds of new data points with 95% confidence when a separate replicate experiment is to be performed. Simulation results show that the model captures the trend of faster NO₂⁻ reduction with increasing flow rates. However, with a single fitting parameter, k_{wt} model profiles are slightly lower than experimental profiles at 1 mL min⁻¹, slightly higher at 40 mL min⁻¹, and approximately match much of the data at the two intermediate flow rates. The reasons for these small discrepancies are unclear, and may be due to nonideal flow in the reactor.

The best-fit intrinsic reaction rate constant (k_w) obtained from the model fit of the data is 5.2×10^{-6} m s⁻¹, and the corresponding dimensionless reaction rate constant (K_w) is 1.3. Nusselt numbers (Nu) and overall dimensionless reaction rate constants (K_E) were calculated at each of the four flow rates with the largest \overline{x} corresponding to x equal to electrode length, L; results are presented in Table 3. This value of \overline{x} was chosen because Nu decreases with increasing \overline{x} and asymptotically approaches a constant value. At all four flow rates, Nu is greater than K_w indicating that NO_2^- reduction in the reactor

Table 3. Summary of Calculated K_w , Nu, and K_E for Nitrite Reduction at Different Flow Rates Using the Reactive Transport Model

flow rate (mL min ⁻¹)	$K_{ m w}$	Nu	$K_{ m E}$
1	1.3	1.4	0.66
5	1.3	2.0	0.78
20	1.3	3.2	0.91
40	1.3	4.5	0.99

is more kinetically limited rather than mass transfer limited. This is more apparent at higher flow rates, where this ratio is greater. For example, while $K_{\rm w}$ is 1.3 for all flow rates, Nu is 1.4 at 1 mL min⁻¹ and 4.5 at 40 mL min⁻¹, respectively. It is important to note however that in all cases Nu is not much greater than $K_{\rm w}$. Hence, mass transfer limitations still affect overall reaction rates and there is room for improvement.

3.4. Reactive Transport Model Application for Improved Reactor Design. The reactive transport model was used to assess the effects of electrode length and width, flow channel thickness, and intrinsic reaction rate constant on NO₂⁻ removal. Results are presented in Figure 6. Electrode length and width had the same effect on NO₂⁻ removal (Figure 6a). Increasing their values by five times sharply increased NO₂⁻ removal from 51% to 96%; the latter corresponds to a final NO₂⁻ concentration close to the U.S. EPA's maximum contaminant level (MCL) of 1 mg L⁻¹ as nitrogen. To probe the effect of flow channel thickness, we adjusted electrode width while varying the thickness to ensure constant retention time and eliminate its effect on NO₂⁻ removal. Both NO₂⁻

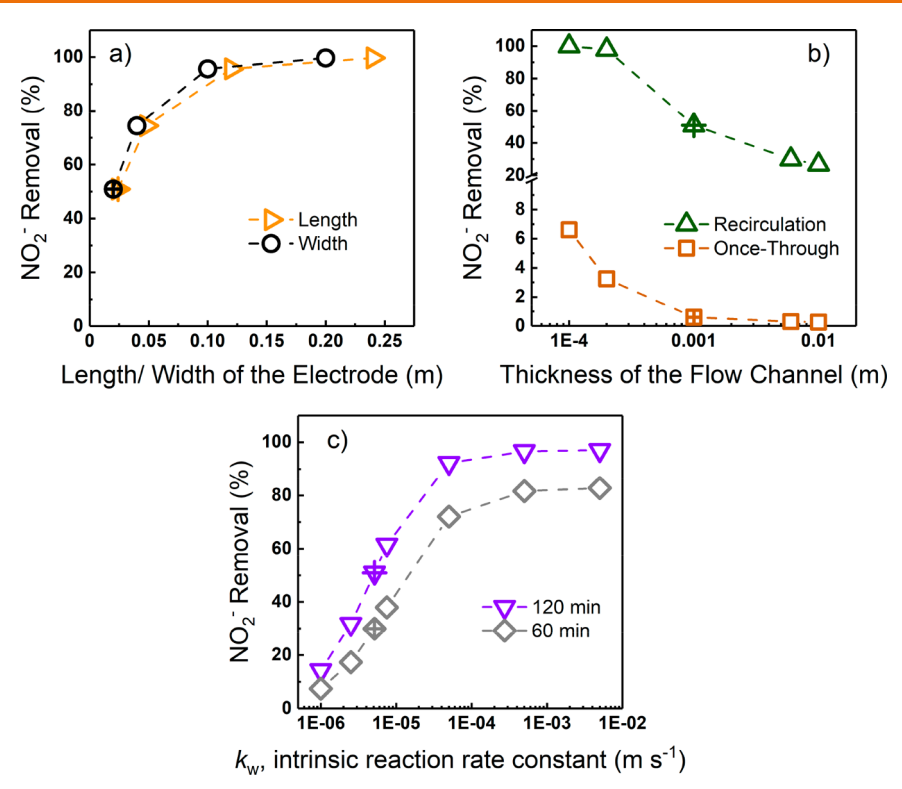


Figure 6. Effect of (a) the length and width of the electrode and (b) the thickness of the flow channel on the NO_2^- removal at 120 min, and (c) effect of the intrinsic reaction rate constant on the NO_2^- removal at 60 and 120 min. Open symbols with "+" signs in the middle represent the NO_2^- removal calculated from the parameters used in the experiments.

I

removal with recirculation and once-through removal (the removal after the solution passes through the reactor once) were evaluated. Results show that $\mathrm{NO_2}^-$ removal for both cases share a similar decreasing trend with increasing flow channel thickness, and that this removal plateaus when flow channel thickness is greater than 0.006 m (Figure 6b). Since the boundary layer thickness is calculated to be 0.006 m, reducing flow channel thickness from 0.006 to 0.0001 m means the flow is cutting into the boundary layer, resulting in a shorter distance for mass transfer, and therefore, a higher removal in both once-through and recirculating modes.

The effects of increasing or decreasing the intrinsic reaction rate constant (k_w) are shown in Figure 6c. As expected, NO₂⁻ removal increases with k_w , but reaches a limiting value at the upper end. Further increases in k_w have little effect past this limit because the overall reaction becomes mass transfer limited at large values of k_w . However, when the overall reaction is mass transfer limited, the value of k_w is 10 times the optimal value determined in this work (shown by the + symbol in Figure 6c). This suggests overall reactor performance may be improved by designing more active catalysts.

We also investigated the effect of flow rate on NO₂⁻ removal using the reactive transport model (Figure S5). When the retention time of fluid in the catalytic reactor is held constant (Figure S5a), once-through NO₂⁻ removals are the same at all flow rates, while removals in the recirculating system increase with flow rate. With a greater number of recirculation events per unit time, the reactor system approaches a more batch-like configuration. When retention time is not held constant (i.e., only flow rate is changing, Figure S5b), once-through NO₂⁻ removals decrease with increasing flow rates; this opposes what boundary layer theory predicts, and is due to the controlling effects of shorter retention times at higher flow rates. By

contrast, in the recirculating system, NO_2^- removal increases with increasing flow rate. The effect of faster recirculation outweighs the disadvantage of shorter retention times. This matches well with the trend of enhanced NO_2^- removal with greater flow rate observed in the experiments from 1 to 40 mL min⁻¹.

3.5. Long-Term Reactor Performance. The same pieces of cathode and stainless steel were used in all reactor experiments. There was concern that reactivity might degrade over time due to alteration of these materials, especially for the Pd–In/ACC cathode. Therefore, at periodic intervals between unique NO₂⁻ reduction experiments performed at different applied potentials and/or flow rates, the same reduction experiment at -1.0 V/RE and 40 mL min⁻¹ was performed seven different times. In total, almost 50 two-hour reduction experiments were performed among unique and replicate experiments, which corresponds to 100 h of reactor operation over six months.

The apparent rate constants for the seven replicate tests are shown in Figure 7. Overall, there is a trend of slightly decreasing activity over time, by approximately 30% from start to finish despite one outlier for test #6. Current efficiency and energy consumption are relatively constant for the seven replicate experiments. The reason for the outlier is possibly a very low potential (-1.5 V/RE) applied in a probe experiment prior to test #6, and the concomitant H₂ gas production that caused some regeneration of the catalyst surface. Pd-based catalysts with various formulations have been shown to continually lose activity over repeated cycles of catalytic nitrate or nitrite reduction, even though no major changes in physical characterizations were observed. Heating the electrodes at moderate temperature in H₂ flow might help restore the activity. Previous long-term studies in catalytic process also

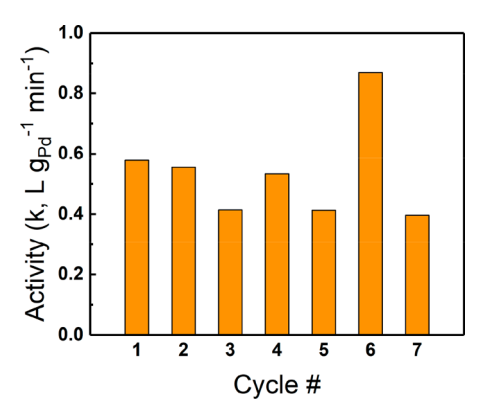


Figure 7. Apparent pseudo-first-order rate constants for multiple cycles of electrocatalytic nitrite reduction at an applied potential of -1.0 V/RE and a flow rate of 40 mL min⁻¹ in the PPTL reactor.

indicated the activity would eventually reach a steady state. ¹⁶ Future studies about whether these observations for Pd catalysts in catalytic reduction are transferable to electroreduction are warranted. This reactor is still promising for application where long-term catalyst activity, efficient hydrogen usage, and low maintenance costs are necessary to achieve sustainability.

3.6. Environmental Implications. Results in this work indicate the PPTL flow reactor promotes rapid NO_2^- reduction at rates commensurate with those in batch reactors, and that mass transfer limitations are not dominating performance. They also indicate that rapid NO_2^- reduction can be achieved with high current efficiency, low energy consumption and excellent selectivity for the dinitrogen end product at a low overpotential where atomic hydrogen is likely responsible for nitrite reduction, and direct charge transfer has little contribution. This bodes well for practice, because that latter mechanism is often associated with high overpotentials and/or H_2 gas evolution, resulting in inefficient use of electricity, high energy consumption, and more corrosion of reactor components.

Modeling results from this work indicate possible approaches to further improve PPTL flow reactor performance. To overcome remaining mass transfer limitations, flow channel thickness could be further reduced or turbulent promoter sheets could be installed to minimize the boundary layer thickness. To enhance hydrogenation rates, more active catalyst formulations can be evaluated. For example, Pd-based alloy nanoparticles (NPs) have shown increased activity toward nitrite reduction. 53,64,75 A remaining challenge not explored by the model is designing a PPTL reactor for largescale application that operated in potentiostatic mode, as opposed to galvanostatic mode. This requires the installation of a reference electrode in a suitable position in a large-scale reactor, which can be difficult. The reference electrode might also be subject to more challenging conditions in practice than at the bench scale, and this might be costly to maintain and operate. Hence, challenges to realize practical implementation of a flow-through electrocatalytic reactor for nitrate removal remain, but promising results from this work regarding high nitrite reduction activity and minimal mass transfer limitations motivate continued development.

ASSOCIATED CONTENT

Supporting Information

The Supporting Information is available free of charge at https://pubs.acs.org/doi/10.1021/acsestengg.0c00054.

Additional materials and methods (page S3–S6); apparent pseudo-first-order rate constants and solution pH of electrocatalytic NO_2^- in different buffer solutions (Table S1); summary of rate constants for (electro)-catalytic NO_2^- reduction in the literature (Table S2); NO_2^- concentration vs time of electrocatalytic NO_2^- reduction in different buffer solutions (Figure S1); reduction current vs time of electrocatalytic NO_2^- reduction at different potentials (Figure S2); NO_2^- reduction rate constants using ACC and Pd-In/ACC (Figure S3); NO_2^- reduction rate constants at 100 mL min $^{-1}$ using a new piece of Pd-In/ACC (Figure S4); model results for the effect of flow rates on NO_2^- removal (Figure S5) (PDF)

AUTHOR INFORMATION

Corresponding Author

Charles J. Werth — Department of Civil, Architectural and Environmental Engineering, The University of Texas at Austin, Austin, Texas 78712, United States; ⊚ orcid.org/0000-0002-8492-5523; Email: werth@utexas.edu

Authors

Chenxu Yan — Department of Civil, Architectural and Environmental Engineering, The University of Texas at Austin, Austin, Texas 78712, United States; orcid.org/0000-0002-2227-5510

Sruthi Kakuturu – Department of Civil, Architectural and Environmental Engineering, The University of Texas at Austin, Austin, Texas 78712, United States

Ashley Hesterberg Butzlaff – Department of Civil and Environmental Engineering, 4105 Seamans Center for the Engineering Arts and Sciences, The University of Iowa, Iowa City, Iowa 52242, United States

David M. Cwiertny — Department of Civil and Environmental Engineering, 4105 Seamans Center for the Engineering Arts and Sciences and Department of Chemical and Biochemical Engineering, 4133 Seamans Center for the Engineering Arts and Sciences, The University of Iowa, Iowa City, Iowa 52242, United States; orcid.org/0000-0001-6161-731X

Syed Mubeen — Department of Chemical and Biochemical Engineering, 4133 Seamans Center for the Engineering Arts and Sciences, The University of Iowa, Iowa City, Iowa 52242, United States

Complete contact information is available at: https://pubs.acs.org/10.1021/acsestengg.0c00054

Notes

The authors declare no competing financial interest.

ACKNOWLEDGMENTS

This work is supported by the Process Systems, Reaction Engineering and Molecular Thermodynamics program of the National Science Foundation under the award numbers CBET-1706797 and 1705255. We thank Jacob P. Troutman from the University of Texas at Austin for taking the TEM image. We also thank Hongyu Guo from the University of

Texas at Austin for calculating the specific area of Pd on the Pd-In/ACC.

REFERENCES

- (1) National Primary Drinking Water Regulations Complete Table; EPA 816-F-09-004; U.S. Environmental Protection Agency, 2009.
- (2) Avery, A. A. Infantile Methemoglobinemia: Reexamining the Role of Drinking Water Nitrates. *Environ. Health Perspect.* **1999**, 107 (7), 583–586.
- (3) Wolff, I. A.; Wasserman, A. E. Nitrates, Nitrites, and Nitrosamines. *Science* **1972**, *177* (4043), 15–19.
- (4) Vorlop, K.-D.; Tacke, T. Erste Schritte Auf Dem Weg Zur Edelmetallkatalysierten Nitrat- Und Nitrit-Entfernung Aus Trinkwasser. *Chem. Ing. Tech.* **1989**, *61* (10), 836–837.
- (5) Chaplin, B. P.; Reinhard, M.; Schneider, W. F.; Schüth, C.; Shapley, J. R.; Strathmann, T. J.; Werth, C. J. Critical Review of Pd-Based Catalytic Treatment of Priority Contaminants in Water. *Environ. Sci. Technol.* **2012**, *46* (7), 3655–3670.
- (6) Martinez, J.; Ortiz, A.; Ortiz, I. State-of-the-Art and Perspectives of the Catalytic and Electrocatalytic Reduction of Aqueous Nitrates. *Appl. Catal.*, B **2017**, 207, 42–59.
- (7) Prüsse, U.; Vorlop, K.-D. Supported Bimetallic Palladium Catalysts for Water-Phase Nitrate Reduction. *J. Mol. Catal. A: Chem.* **2001**, *173* (1), 313–328.
- (8) Hörold, S.; Tacke, T.; Vorlop, K.-D. Catalytical Removal of Nitrate and Nitrite from Drinking Water: 1. Screening for Hydrogenation Catalysts and Influence of Reaction Conditions on Activity and Selectivity. *Environ. Technol.* 1993, 14 (10), 931–939.
- (9) Strukul, G.; Gavagnin, R.; Pinna, F.; Modaferri, E.; Perathoner, S.; Centi, G.; Marella, M.; Tomaselli, M. Use of Palladium Based Catalysts in the Hydrogenation of Nitrates in Drinking Water: From Powders to Membranes. *Catal. Today* **2000**, *55* (1), 139–149.
- (10) Prüsse, U.; Hähnlein, M.; Daum, J.; Vorlop, K.-D. Improving the Catalytic Nitrate Reduction. Catal. Today 2000, 55 (1), 79–90.
- (11) Shuai, D.; Choe, J. K.; Shapley, J. R.; Werth, C. J. Enhanced Activity and Selectivity of Carbon Nanofiber Supported Pd Catalysts for Nitrite Reduction. *Environ. Sci. Technol.* **2012**, *46* (5), 2847–2855.
- (12) Yoshinaga, Y.; Akita, T.; Mikami, I.; Okuhara, T. Hydrogenation of Nitrate in Water to Nitrogen over Pd-Cu Supported on Active Carbon. *J. Catal.* **2002**, *207* (1), 37–45.
- (13) Pintar, A.; Batista, J. Catalytic Hydrogenation of Aqueous Nitrate Solutions in Fixed-Bed Reactors. *Catal. Today* **1999**, *53* (1), 35–50.
- (14) Pintar, A.; Batista, J. Catalytic Stepwise Nitrate Hydrogenation in Batch-Recycle Fixed-Bed Reactors. *J. Hazard. Mater.* **2007**, *149* (2), 387–398.
- (15) Pintar, A.; Batista, J. Improvement of an Integrated Ion-Exchange/Catalytic Process for Nitrate Removal by Introducing a Two-Stage Denitrification Step. *Appl. Catal., B* **2006**, *63* (1), 150–159.
- (16) Bergquist, A. M.; Choe, J. K.; Strathmann, T. J.; Werth, C. J. Evaluation of a Hybrid Ion Exchange-Catalyst Treatment Technology for Nitrate Removal from Drinking Water. *Water Res.* **2016**, *96*, 177–187.
- (17) Choe, J. K.; Bergquist, A. M.; Jeong, S.; Guest, J. S.; Werth, C. J.; Strathmann, T. J. Performance and Life Cycle Environmental Benefits of Recycling Spent Ion Exchange Brines by Catalytic Treatment of Nitrate. *Water Res.* **2015**, *80*, 267–280.
- (18) Marchesini, F. A.; Mendow, G.; Picard, N. P.; Zoppas, F. M.; Aghemo, V. S.; Gutierrez, L. B.; Querini, C. A.; Miró, E. E. PdIn Catalysts in a Continuous Fixed Bed Reactor for the Nitrate Removal from Groundwater. *Int. J. Chem. React. Eng.* **2019**, DOI: 10.1515/ijcre-2018-0126.
- (19) Mendow, G.; Marchesini, F. A.; Miró, E. E.; Querini, C. A. Evaluation of Pd-In Supported Catalysts for Water Nitrate Abatement in a Fixed-Bed Continuous Reactor. *Ind. Eng. Chem. Res.* **2011**, *50* (4), 1911–1920.
- (20) Bergquist, A. M.; Bertoch, M.; Gildert, G.; Strathmann, T. J.; Werth, C. J. Catalytic Denitrification in a Trickle Bed Reactor: Ion

- Exchange Waste Brine Treatment. J. Am. Water Works Assoc. 2017, 109 (5), E129-E151.
- (21) Bertoch, M.; Bergquist, A. M.; Gildert, G.; Strathmann, T. J.; Werth, C. J. Catalytic Nitrate Removal in a Trickle Bed Reactor: Direct Drinking Water Treatment. J. Am. Water Works Assoc. 2017, 109 (5), E144–E171.
- (22) Lüdtke, K.; Peinemann, K.-V.; Kasche, V.; Behling, R.-D. Nitrate Removal of Drinking Water by Means of Catalytically Active Membranes. J. Membr. Sci. 1998, 151 (1), 3–11.
- (23) Hähnlein, M.; Prüße, U.; Daum, J.; Morawsky, V.; Kröger, M.; Schröder, M.; Schnabel, M.; Vorlop, K.-D. Preparation of Microscopic Catalysts and Colloids for Catalytic Nitrate and Nitrite Reduction and Their Use in a Hollow Fibre Dialyser Loop Reactor. *Stud. Surf. Sci. Catal.* 1998, 118, 99–107.
- (24) Marks, R.; Seaman, J.; Perez-Calleja, P.; Kim, J.; Nerenberg, R.; Doudrick, K. Catalytic Hydrogel Membrane Reactor for Treatment of Aqueous Contaminants. *Environ. Sci. Technol.* **2019**, 53 (11), 6492–6500.
- (25) Brunet Espinosa, R.; Rafieian, D.; Postma, R. S.; Lammertink, R. G. H.; Lefferts, L. Egg-Shell Membrane Reactors for Nitrite Hydrogenation: Manipulating Kinetics and Selectivity. *Appl. Catal., B* **2018**, 224, 276–282.
- (26) Gao, J.; Jiang, B.; Ni, C.; Qi, Y.; Bi, X. Enhanced Reduction of Nitrate by Noble Metal-Free Electrocatalysis on P Doped Three-Dimensional Co3O4 Cathode: Mechanism Exploration from Both Experimental and DFT Studies. *Chem. Eng. J.* **2020**, 382, 123034.
- (27) Mácová, Z.; Bouzek, K.; Šerák, J. Electrocatalytic Activity of Copper Alloys for NO3-reduction in a Weakly Alkaline Solution. *J. Appl. Electrochem.* **2007**, 37 (5), 557–566.
- (28) Katsounaros, I.; Ipsakis, D.; Polatides, C.; Kyriacou, G. Efficient Electrochemical Reduction of Nitrate to Nitrogen on Tin Cathode at Very High Cathodic Potentials. *Electrochim. Acta* **2006**, 52 (3), 1329–1338.
- (29) Bouzek, K.; Paidar, M.; Sadílková, A.; Bergmann, H. Electrochemical Reduction of Nitrate in Weakly Alkaline Solutions. *J. Appl. Electrochem.* **2001**, *31* (11), 1185–1193.
- (30) Garcia-Segura, S.; Lanzarini-Lopes, M.; Hristovski, K.; Westerhoff, P. Electrocatalytic Reduction of Nitrate: Fundamentals to Full-Scale Water Treatment Applications. *Appl. Catal., B* **2018**, 236, 546–568.
- (31) Petrii, O. A.; Safonova, T. Ya Electroreduction of Nitrate and Nitrite Anions on Platinum Metals: A Model Process for Elucidating the Nature of the Passivation by Hydrogen Adsorption. *J. Electroanal. Chem.* **1992**, 331 (1), 897–912.
- (32) Safonova, T. Y.; Petrii, O. A. Effect of Inorganic Cations on the Electroreduction of Nitrate Anions on PtlPt Electrodes in Sulfuric Acid Solutions1This Paper Is Dedicated to Professor A. Despic in Honour of His 70th Birthday.1. *J. Electroanal. Chem.* 1998, 448 (2), 211–216.
- (33) Petrii, O. A.; Akbaeva, Y. A.; Safonova, T. Y.; Kondrasheva, V. S.; Kolosov, E. N.; Tsirlina, G. A.; Gryaznov, V. M. Intensification of the Nitrate Anion Reduction on a Membrane Palladium Electrode. *Russ. J. Electrochem.* **2002**, 38 (2), 220–223.
- (34) Lu, C.; Lu, S.; Qiu, W.; Liu, Q. Electroreduction of Nitrate to Ammonia in Alkaline Solutions Using Hydrogen Storage Alloy Cathodes. *Electrochim. Acta* **1999**, 44 (13), 2193–2197.
- (35) Pletcher, D.; Walsh, F. C. Electrochemical Engineering. In *Industrial Electrochemistry*; Pletcher, D., Walsh, F. C., Eds.; Springer Netherlands: Dordrecht, 1993; pp 60–172. DOI: 10.1007/978-94-011-2154-5_2.
- (36) Reyter, D.; Bélanger, D.; Roué, L. Optimization of the Cathode Material for Nitrate Removal by a Paired Electrolysis Process. *J. Hazard. Mater.* **2011**, 192 (2), 507–513.
- (37) Paidar, M.; Roušar, I.; Bouzek, K. Electrochemical Removal of Nitrate Ions in Waste Solutions after Regeneration of Ion Exchange Columns. *J. Appl. Electrochem.* **1999**, 29 (5), 611–617.
- (38) Paidar, M.; Bouzek, K.; Bergmann, H. Influence of Cell Construction on the Electrochemical Reduction of Nitrate. *Chem. Eng. J.* **2002**, 85 (2), 99–109.

- (39) Ding, J.; Li, W.; Zhao, Q.-L.; Wang, K.; Zheng, Z.; Gao, Y.-Z. Electroreduction of Nitrate in Water: Role of Cathode and Cell Configuration. *Chem. Eng. J.* **2015**, *271*, 252–259.
- (40) Szpyrkowicz, L.; Daniele, S.; Radaelli, M.; Specchia, S. Removal of NO3- from Water by Electrochemical Reduction in Different Reactor Configurations. *Appl. Catal., B* **2006**, *66* (1), 40–50.
- (41) Bockris, J. O.; Kim, J. Electrochemical Treatment of Low-Level Nuclear Wastes. *J. Appl. Electrochem.* **1997**, 27 (6), 623–634.
- (42) Kim, H.-K.; Jeong, J.-Y.; Cho, H.-N.; Park, J.-Y. Kinetics of Nitrate Reduction with the Packed Bed Iron Bipolar Electrode. *Sep. Purif. Technol.* **2015**, *152*, 140–147.
- (43) Gayen, P.; Spataro, J.; Avasarala, S.; Ali, A.-M.; Cerrato, J. M.; Chaplin, B. P. Electrocatalytic Reduction of Nitrate Using Magnéli Phase TiO2 Reactive Electrochemical Membranes Doped with Pd-Based Catalysts. *Environ. Sci. Technol.* **2018**, *52* (16), 9370–9379.
- (44) Rivera, F. F.; de León, C. P.; Nava, J. L.; Walsh, F. C. The Filter-Press FM01-LC Laboratory Flow Reactor and Its Applications. *Electrochim. Acta* **2015**, *163*, 338–354.
- (45) Hasnat, M. A.; Ishibashi, I.; Sato, K.; Agui, R.; Yamaguchi, T.; Ikeue, K.; Machida, M. Electrocatalytic Reduction of Nitrate Using Cu-Pd and Cu-Pt Cathodes/H+-Conducting Solid Polymer Electrolyte Membrane Assemblies. *Bull. Chem. Soc. Jpn.* **2008**, *81* (12), 1675–1680.
- (46) Machida, M.; Sato, K.; Ishibashi, I.; Hasnat, M. A.; Ikeue, K. Electrocatalytic Nitrate Hydrogenation over an H+-Conducting Solid Polymer Electrolyte Membrane-Modified Cathode Assembly. *Chem. Commun.* **2006**, No. 7, 732–734.
- (47) Hasnat, M. A.; Ben Aoun, S.; Rahman, M. M.; Asiri, A. M.; Mohamed, N. Lean Cu-Immobilized Pt and Pd Films/-H+Conducting Membrane Assemblies: Relative Electrocatalytic Nitrate Reduction Activities. *J. Ind. Eng. Chem.* **2015**, *28*, 131–137.
- (48) Cheng, H.; Scott, K.; Christensen, P. A. Application of a Solid Polymer Electrolyte Reactor to Remove Nitrate Ions from Wastewater. *J. Appl. Electrochem.* **2005**, 35 (6), 551–560.
- (49) Jha, K.; Weidner, J. W. Evaluation of Porous Cathodes for the Electrochemical Reduction of Nitrates and Nitrites in Alkaline Waste Streams. *J. Appl. Electrochem.* **1999**, 29 (11), 1305–1315.
- (50) Genders, J. D.; Hartsough, D.; Hobbs, D. T. Electrochemical Reduction of Nitrates and Nitrites in Alkaline Nuclear Waste Solutions. J. Appl. Electrochem. 1996, 26 (1), 1–9.
- (51) Chaplin, B. P.; Shapley, J. R.; Werth, C. J. Regeneration of Sulfur-Fouled Bimetallic Pd-Based Catalysts. *Environ. Sci. Technol.* **2007**, *41* (15), 5491–5497.
- (52) Chae, K. J.; Choi, M.; Ajayi, F. F.; Park, W.; Chang, I. S.; Kim, I. S. Mass Transport through a Proton Exchange Membrane (Nafion) in Microbial Fuel Cells. *Energy Fuels* **2008**, 22 (1), 169–176.
- (53) Seraj, S.; Kunal, P.; Li, H.; Henkelman, G.; Humphrey, S. M.; Werth, C. J. PdAu Alloy Nanoparticle Catalysts: Effective Candidates for Nitrite Reduction in Water. ACS Catal. 2017, 7 (5), 3268–3276.
- (54) Gao, D.; Zhou, H.; Wang, J.; Miao, S.; Yang, F.; Wang, G.; Wang, J.; Bao, X. Size-Dependent Electrocatalytic Reduction of CO2 over Pd Nanoparticles. *J. Am. Chem. Soc.* **2015**, *137* (13), 4288–4291.
- (55) Jiang, B.; Zhang, X.-G.; Jiang, K.; Wu, D.-Y.; Cai, W.-B. Boosting Formate Production in Electrocatalytic CO2 Reduction over Wide Potential Window on Pd Surfaces. *J. Am. Chem. Soc.* **2018**, *140* (8), 2880–2889.
- (56) Gidaspow, D. Convective Diffusion in a Parallel Plate Duct with One Catalytic Wall Laminar Flow First Order Reaction Part I Analytical. *Can. J. Chem. Eng.* **1967**, 45 (1), 35–39.
- (57) Solbrig, C. W. Convective Diffusion in a Rectangular Duct with One Catalytic Wall. Ph.D. Thesis, Illinois Institute of Technology: Ann Arbor, MI, 1966.
- (58) Marchesini, F. A.; Irusta, S.; Querini, C.; Miró, E. Nitrate Hydrogenation over Pt,In/Al2O3 and Pt,In/SiO2. Effect of Aqueous Media and Catalyst Surface Properties upon the Catalytic Activity. *Catal. Commun.* **2008**, *9* (6), 1021–1026.
- (59) Misal, S. N.; Lin, M.-H.; Mehraeen, S.; Chaplin, B. P. Modeling Electrochemical Oxidation and Reduction of Sulfamethoxazole Using

- Electrocatalytic Reactive Electrochemical Membranes. J. Hazard. Mater. 2020, 384, 121420.
- (60) Hasnat, M. A.; Agui, R.; Hinokuma, S.; Yamaguchi, T.; Machida, M. Different Reaction Routes in Electrocatalytic Nitrate/Nitrite Reduction Using an H+-Conducting Solid Polymer Electrolyte. *Catal. Commun.* **2009**, *10* (7), 1132–1135.
- (61) Hasnat, M. A.; Karim, M. R.; Machida, M. Electrocatalytic Ammonia Synthesis: Role of Cathode Materials and Reactor Configuration. *Catal. Commun.* **2009**, *10* (15), 1975–1979.
- (62) Brylev, O.; Sarrazin, M.; Roué, L.; Bélanger, D. Nitrate and Nitrite Electrocatalytic Reduction on Rh-Modified Pyrolytic Graphite Electrodes. *Electrochim. Acta* **2007**, 52 (21), 6237–6247.
- (63) Chaplin, B. P.; Roundy, E.; Guy, K. A.; Shapley, J. R.; Werth, C. J. Effects of Natural Water Ions and Humic Acid on Catalytic Nitrate Reduction Kinetics Using an Alumina Supported Pd-Cu Catalyst. *Environ. Sci. Technol.* **2006**, *40* (9), 3075–3081.
- (64) Guy, K. A.; Xu, H.; Yang, J. C.; Werth, C. J.; Shapley, J. R. Catalytic Nitrate and Nitrite Reduction with Pd-Cu/PVP Colloids in Water: Composition, Structure, and Reactivity Correlations. *J. Phys. Chem. C* **2009**, *113* (19), 8177–8185.
- (65) de Vooys, A. C. A.; van Santen, R. A.; van Veen, J. A. R. Electrocatalytic Reduction of NO3- on Palladium/Copper Electrodes. *J. Mol. Catal. A: Chem.* **2000**, *154* (1), 203–215.
- (66) Shin, H.; Jung, S.; Bae, S.; Lee, W.; Kim, H. Nitrite Reduction Mechanism on a Pd Surface. *Environ. Sci. Technol.* **2014**, 48 (21), 12768–12774.
- (67) Prüsse, U.; Daum, J.; Bock, C.; Vorlop, K.-D. Catalytic Nitrate Reduction: Kinetic Investigations. *Stud. Surf. Sci. Catal.* **2000**, *130*, 2237–2242.
- (68) Pintar, A.; Setinc, M.; Levec, J. Hardness and Salt Effects on Catalytic Hydrogenation of Aqueous Nitrate Solutions. *J. Catal.* **1998**, 174 (1), 72–87.
- (69) Huo, X.; Van Hoomissen, D. J.; Liu, J.; Vyas, S.; Strathmann, T. J. Hydrogenation of Aqueous Nitrate and Nitrite with Ruthenium Catalysts. *Appl. Catal., B* **2017**, *211*, 188–198.
- (70) Li, H.; Yan, C.; Guo, H.; Shin, K.; Humphrey, S. M.; Werth, C. J.; Henkelman, G. CuxIr1-x Nanoalloy Catalysts Achieve Near 100% Selectivity for Aqueous Nitrite Reduction to NH3. *ACS Catal.* **2020**, *10*, 7915.
- (71) Georgeaud, V.; Diamand, A.; Borrut, D.; Grange, D.; Coste, M. Electrochemical Treatment of Wastewater Polluted by Nitrate: Selective Reduction to N2 on Boron-Doped Diamond CathodeV. Georgeaud et al. Electrochemical Treatment of Wastewater Polluted by Nitrate. *Water Sci. Technol.* **2011**, *63* (2), 206–212.
- (72) Lacasa, E.; Cañizares, P.; Llanos, J.; Rodrigo, M. A. Removal of Nitrates by Electrolysis in Non-Chloride Media: Effect of the Anode Material. *Sep. Purif. Technol.* **2011**, *80* (3), 592–599.
- (73) Abdallah, R.; Geneste, F.; Labasque, T.; Djelal, H.; Fourcade, F.; Amrane, A.; Taha, S.; Floner, D. Selective and Quantitative Nitrate Electroreduction to Ammonium Using a Porous Copper Electrode in an Electrochemical Flow Cell. *J. Electroanal. Chem.* **2014**, 727, 148–153.
- (74) Clark, M. M. Transport Modeling for Environmental Engineers and Scientists, 2nd ed..; John Wiley & Sons, 2011.
- (75) Troutman, J. P.; Li, H.; Haddix, A. M.; Kienzle, B. A.; Henkelman, G.; Humphrey, S. M.; Werth, C. J. PdAg Alloy Nanocatalysts: Toward Economically Viable Nitrite Reduction in Drinking Water. *ACS Catal.* **2020**, *10* (14), 7979–7989.
- (76) Werth, C. J.; Yan, C.; Troutman, J. P. Factors Impeding Replacement of Ion Exchange with (Electro)Catalytic Treatment for Nitrate Removal from Drinking Water. ACS EST Eng. 2020, DOI: 10.1021/acsestengg.0c00076.